European Journal of Mechanics B/Fluids 29 (2010) 1–8

Contents lists available at ScienceDirect

European Journal of Mechanics B/Fluids

journal homepage: www.elsevier.com/locate/ejmflu

On the origin of spin-up processes in decaying two-dimensional turbulence

G.H. Keetels [a], H.J.H. Clercx [a, b, *], G.J.F. van Heijst [a]

[a] Department of Physics, Eindhoven University of Technology, P.O. Box 513, 5600 MB Eindhoven, The Netherlands
[b] Department of Applied Mathematics, University of Twente, P.O. Box 217, 7500 AE Enschede, The Netherlands

ARTICLE INFO

Article history:
Received 25 January 2009
Received in revised form
18 June 2009
Accepted 18 June 2009
Available online 30 June 2009

PACS:
47.27.De
47.27.E–
47.27.ek
47.32.C–

Keywords:
2D turbulence
No-slip boundaries
Spontaneous spin-up
Angular momentum
Volume penalization

ABSTRACT

A remarkable feature of two-dimensional turbulence in a square container with no-slip walls is the spontaneous production of angular momentum due to flow-wall interactions, also known as spontaneous spin-up of the flow. In this paper we address the statistics of spin-up and discuss its likely origin. A signature of the spontaneous production of angular momentum is the development of a large-scale circulation cell. It is found that the global turnover time of the flow guides the spin-up process, which can be considered as a relaxation process of the macroscopic flow to an angular momentum containing state. The high turnover rate of the small-scale vortical structures emerging from the no-slip walls apparently has no significant effect on the spin-up rate. The presented data on the spin-up process strongly suggest that spin-up is not the net result of isolated vortex-wall interactions, with its associated pressure fluctuations on the domain boundaries, alone. The rapid spin-up of the flow clearly suggests the attraction to an angular momentum containing state.

1. Introduction

The remarkable features of self-organizing two-dimensional (2D) flows have been studied since the pioneering analysis of Kraichnan [1], Batchelor [2] and Leith [3]. In contrast to three-dimensional turbulence two-dimensional flows have a tendency of self-organization due to the presence of the inverse energy cascade, *i.e.* the kinetic energy condenses in the largest scale available. Simultaneously, the enstrophy is transferred downscale towards the viscous dissipation range. The inverse cascade is clearly observed in forced 2D turbulence, but it should be noted that, depending on the choice of the initial condition, it might be less prominently present in decaying 2D turbulence. The formation of large scales might then also be interpreted in terms of selective decay [4]. Most theoretical studies, including the classical works of Kraichnan, Batchelor and Leith, consider isotropic and homogeneous turbulence. The main reason for this approach is the conjecture that 2D turbulent flows, provided they are sufficiently well separated from the domain boundaries, are statistically isotropic and homogeneous. In numerical studies homogeneity and isotropy conditions can be satisfied when periodic boundary conditions are applied. This choice for the boundary condition is also motivated by the availability of parallel fast Fourier spectral solvers.

The effect of the presence of solid (no-slip) walls on the properties of decaying two-dimensional flows turned out to be of crucial importance. For a recent overview, see Refs. [5,6]. In particular, the end-state of decaying 2D turbulence is strikingly different for flow in a periodic domain and a domain confined by solid walls. The quasi-stationary final state of decaying turbulence on a periodic domain is in most cases a large-scale dipole. However, also a so-called 'bar-state' has been found as a quasi-stationary final state [7]. The experiments and numerical simulations of decaying 2D turbulence at moderate integral-scale Reynolds numbers on a square bounded domain reported by Clercx et al. [8,9] and Maassen et al. [10] have shown that the flow at moderate Reynolds numbers can spontaneously produce angular momentum. This process starts early in the decay process and results in the formation of a domain-sized monopolar or tripolar vortex structure. For flows that are confined by circular no-slip walls, first studied

* Corresponding author. Department of Physics, Eindhoven University of Technology, P.O. Box 513, 5600 MB Eindhoven, The Netherlands. Tel.: +31 402472680; fax: +31 402464151.
E-mail address: h.j.h.clercx@tue.nl (H.J.H. Clercx).

0997-7546/$ – see front matter © 2009 Elsevier Masson SAS. All rights reserved.
doi:10.1016/j.euromechflu.2009.06.004

numerically by Li et al. [11–13], the production of angular momentum is virtually absent [12,14]. This observation is also confirmed by the experimental studies of Maassen et al. [10,15]. Recently, it has been shown that the absence of spin-up in a circular geometry can be explained by the role of the pressure on the domain boundaries. For circular domains the pressure does not contribute to the generation of angular momentum. For decaying turbulence in elliptic domains Keetels et al. [16] have observed that the introduction of a small amount of eccentricity, thus rendering the torques by pressure forces effective, can already trigger the spin-up phenomenon. The observation that the pressure on the domain boundaries drives the spin-up suggests that the production of angular momentum will also be an important process for turbulent flow in bounded domains in the limit of infinite Reynolds numbers. In that limit only the pressure forces contribute to the torque as viscous (normal and shear) stresses are then absent (for more details, see Section 2).

High-resolution numerical simulations of 2D turbulence in square domains are here conducted with a 2D Fourier pseudo-spectral method, with the boundary conditions implemented by a volume-penalization method [17]. The purpose of this study is twofold. First, comparison with data from previous simulations with a 2D Chebyshev pseudospectral method [8,9], gives insight in the reliability of the novel method. Second, this new method allows 2D turbulence simulations with initial integral-scale Reynolds numbers at least one order of magnitude larger then reported in previous studies [8,9]. This allows verification of the presence of the spontaneous spin-up phenomenon at significantly higher Reynolds numbers than considered in previous studies of turbulence on square bounded domains. Several characteristics of the spin-up process are determined for high-Reynolds number flow, such as the magnitude of the torque and the strength of the large-scale recirculation cell which results from spin-up. Furthermore, it is examined if a characteristic dimensionless time can be identified for the spin-up of the flow.

The paper is organized as follows. In Section 2 the angular momentum balance and numerical set-up is briefly introduced. The flow phenomenology will be discussed in Section 3 and some statistical data on spin-up will be provided in Sections 4 and 5. Finally, a brief summary is given in Section 6.

2. Angular momentum balance

We consider the 2D motion of an incompressible, viscous fluid on a bounded domain Ω with (no-slip) boundary $\partial\Omega$. An important quantity for fluids on a bounded domain is the angular momentum L associated with the fluid motion. Defining a Cartesian reference frame, with $\boldsymbol{r}=(x, y)$ in the plane of the flow and its origin in the centre of the container, the angular momentum reads

$$L = \int_{\Omega} (\boldsymbol{r}\times\boldsymbol{u})\cdot\boldsymbol{e}_z \, dA = \int_{\Omega} (xv - yu)\, dA, \tag{1}$$

with $\boldsymbol{u}=(u, v)$ the flow field and $\boldsymbol{e}_z$ the unit vector perpendicular to the plane of the flow. By inserting the Navier–Stokes equations in velocity–pressure form into the definition of the time rate of change of the angular momentum it is obtained that,

$$\frac{dL}{dt} = \frac{1}{\rho}\oint_{\partial\Omega} p\boldsymbol{r}\cdot ds + \nu \oint_{\partial\Omega} \omega(\boldsymbol{r}\cdot\boldsymbol{n})\, ds, \tag{2}$$

with ρ the density, p the pressure, ν the kinematic viscosity, and ω the (scalar) vorticity defined by $\omega=\partial v/\partial x-\partial u/\partial y$. Furthermore, $\boldsymbol{n}$ is the unit (outward) normal on the boundary and $d\boldsymbol{s}$ an infinitesimal tangential element of the boundary (and ds its norm). Since the angular momentum can be rewritten in terms of the vorticity, $L = -1/2\int_{\Omega} r^2\omega\, dA$, it is possible to derive an alternative expression by using the vorticity equation,

$$\frac{dL}{dt} = -\frac{1}{2}\nu\oint_{\partial\Omega} r^2(\boldsymbol{n}\cdot\nabla\omega)\, ds + \nu\oint_{\partial\Omega}\omega(\boldsymbol{r}\cdot\boldsymbol{n})\, ds. \tag{3}$$

It can be deduced that the first terms on the right-hand side of (2) and (3) have to balance since the second term on the right-hand side of both expressions is identical. A natural assumption is that the pressure at the boundary will reach a finite value in the limit of infinite Reynolds numbers. This implies that the product $\nu\partial\omega/\partial n$ should be finite as well for vanishing viscosity, thus providing a scaling relation for the normal vorticity gradient at the no-slip boundary: $\partial\omega/\partial n|_{wall}\propto \mathrm{Re}$. Here, $\mathrm{Re}=UL/\nu$ is the Reynolds number, with U and L a typical velocity and length scale. For the vorticity at the wall this implies $\omega|_{wall}\propto\sqrt{\mathrm{Re}}$ [18], underlining the importance of no-slip walls as vorticity sources.

A Fourier spectral method is applied in order to achieve higher-order precision for the internal flow and the flow near the boundaries. The no-slip walls are modelled by means of an immersed boundary technique known as the volume-penalization or Brinkman-penalization method. Inside the domain we solve the usual Navier–Stokes equation and in the volume of the obstacle a Darcy term is added to the Navier–Stokes equation. By making the penalization or permeability parameter sufficiently small one achieves a no-slip condition at the interface between the fluid and the porous solid. This idea originated from Arquis and Caltagirone [19] and was further developed by Angot et al. [20] and by Carbou and Fabrie [21]. In Keetels et al. [17,22] details of the numerical method are discussed and it is shown that the volume-penalization method can successfully be adopted for Fourier spectral methods. Furthermore, the convergence of the scheme is studied by considering dipole-wall collisions. Recently, volume penalization has been applied by Schneider and coworkers in several studies on bounded 2D turbulent fluid and plasma flows [23,24].

The initial condition basically consists of 100 nearly equal-sized Gaussian vortices with a dimensionless radius 0.05 in a domain with a size of 2×2 units. The initial condition is normalized such that the rms velocity $U=1$. This then corresponds with a vortex amplitude $\omega_{max}\simeq 100$. Half of the vortices have positive circulation and the other vortices have negative circulation. The vortices are placed on a regular lattice, well away from the boundaries. The symmetry is slightly broken by a small displacement of the vortex centres and a slight variation of the vortex amplitudes. More details about the initialization procedure as sketched above can be found in Ref. [9]. In Fourier transform space certain coefficients are set equal to zero such that the initial angular momentum is zero within machine precision. A smoothing function, similar to the one employed in Ref. [8], is applied to ensure that the initial flow is consistent with the no-slip boundary condition. The parameters of the simulations are assembled in Table 1.

3. Flow features

Fig. 1 shows several snapshots of the vorticity distribution of decaying flow with an initial Reynolds number of $\mathrm{Re}=10^5$. Time has been made dimensionless with the eddy turnover time of the Gaussian vortices from the initial condition. The vorticity snapshot taken from the vigorous early stage of the turbulent decay process at $\tau=7$ shows several characteristic features such as merging of like-sign vortices in the centre of the container and the formation of medium-sized dipoles. During several collisions of vortex structures with the domain boundaries high-amplitude vorticity filaments are injected into the interior of the flow domain and roll up

Table 1
Overview of the simulations on a square domain. The first column denotes the number of runs in each ensemble. The Reynolds number Re is based on the rms velocity and half-width W of the domain. N denotes the spatial resolution, N_{act} is the number of active Fourier coefficients, ε the penalization parameter and δt the time-step.

No.	Re	N	N_{act}	ϵ	δt
10	10^4	1024	682	10^{-8}	1.0×10^{-4}
5	5×10^4	2048	1364	10^{-8}	5.0×10^{-5}
5	10^5	4096	2730	10^{-8}	2.5×10^{-5}

into new vortex cores. These new small-scale vortices contain high-amplitude vorticity. The second stage of the decay process, for which a typical example of the vorticity distribution is displayed in Fig. 1 at $\tau = 20$, is characterized by the formation of increasingly larger coherent structures. Injection of small-scale vorticity from the no-slip domain boundaries and subsequent formation of new vortex cores continues.

Fig. 2 gives the stream function corresponding with the vorticity fields in Fig. 1. The streamlines reveal the development of a large-scale flow pattern during the decay process. Since the angular momentum can equivalently be expressed in terms of the stream function ψ as $L = 2\int \psi\, dA$ it is obvious that the flow has acquired net angular momentum. This is strikingly different compared to the final state of decaying turbulence on a periodic domain, for which the angular momentum is trivially zero. The (quasi-stationary) final state of the decay process in a periodic box is a large-scale dipolar vortex structure [4]. Under certain circumstances the 'bar-state' is retrieved, see Ref. [7].

The overall picture of the decay process in a no-slip box considered here for $\mathrm{Re} = 10^5$ is similar to the $\mathrm{Re} = 10^4$ case reported in Clercx et al. [9]. An important difference is, however, the presence of a much larger number of (small-scale) vortices in the high-Reynolds number case. The size of these small-scale vortices is substantially less than the size of the Gaussian vortices constituting the initial vorticity field. The diameter of these Gaussian vortices is approximately one-tenth of the container size. To demonstrate that the small-scale vortex structures are indeed the result of flow-wall interaction, a comparison with a numerical simulation on a double periodic domain is shown in Fig. 3. The initial condition and the (initial) Reynolds number for the periodic computation are the same as for the no-slip case. Note the large number of small-scale vortices distributed over the entire square domain (with no-slip walls). Such small-scale vortices are virtually absent in the periodic case. This observation signifies that these vortices are indeed formed due to flow-wall interaction events.

Also in the late-time evolution several differences are discovered between the present results with $\mathrm{Re} = 10^5$ and those with $\mathrm{Re} = 10^4$, reported previously by Clercx et al. [9]. Around $\tau = 200$ a monopolar or a tripolar structure emerges that completely fills the domain for $\mathrm{Re} = 10^4$. For the high-Reynolds number decay process considered here it is observed that the radius of the dominant vortex structure appearing around the same time is significantly smaller. Two processes are responsible for the presence of a smaller dominant vortex in the high-Reynolds number case. First of all it is due to reduced lateral diffusion, which slows down the broadening of the dominant vortex cores. Additionally, the dominant vortex structures merge with on average smaller vortices in the high-Reynolds number runs. Many of these small vortices contain high-amplitude vorticity that originate from detached boundary layers (which become thinner as the Reynolds number increases). Also in the late-time evolution the number of vortices in the high-Reynolds number case is much larger. Note that although the radius of the dominant vortex is smaller, the associated stream function displayed in Fig. 2 reveals the development of a global circulation cell in the interior of the container, which contains net angular momentum.

Fig. 4 shows the total kinetic energy, $E = 1/2\int_\Omega |\mathbf{u}|^2\, dA$, and the enstrophy of the flow, $Z = 1/2\int_\Omega \omega^2\, dA$, versus the dimensionless time τ for several typical runs of decaying turbulence on a square domain with no-slip walls. Fig. 4a and c show the results for $\mathrm{Re} = 10^4$, b and e for $\mathrm{Re} = 5\times10^4$, and c and f for $\mathrm{Re} = 10^5$, respectively. As reference we have plotted the kinetic energy and enstrophy for decaying turbulence on a double periodic domain with $\mathrm{Re} = 10^5$ in Fig. 4c and f, see the dotted lines ($\tau \lesssim 100$). The enstrophy of the flow on a periodic domain, represented by the dotted line in Fig. 4f, decays very rapidly due to the vorticity gradient amplification process (see Ref. [2]). During the vigorous first stage of the decay process on a bounded domain intense production of small-scale vorticity at the domain boundaries occurs which compensates for the enstrophy dissipation (and it even might instantaneously increase the enstrophy of the flow substantially), see Fig. 4e and f. Persistence of enstrophy implies enhanced dissipation of kinetic energy according to $dE/dt = -2Z(t)/\mathrm{Re}$, and the dissipation rate of the total kinetic energy in the no-slip case is significantly faster compared with the periodic case, see Fig. 4c. For decaying turbulence on a periodic domain the enstrophy is bounded by its initial value. This implies that $|dE(t)/dt| \leq 2Z(t=0)/\mathrm{Re}$, thus the energy dissipation rate falls of proportional to Re^{-1} in the periodic case provided $Z(t) \approx Z(t=0)$ (for sufficiently small t). For larger times the energy dissipation rate will inevitably decrease as the enstrophy is a monotonically decaying function of time.

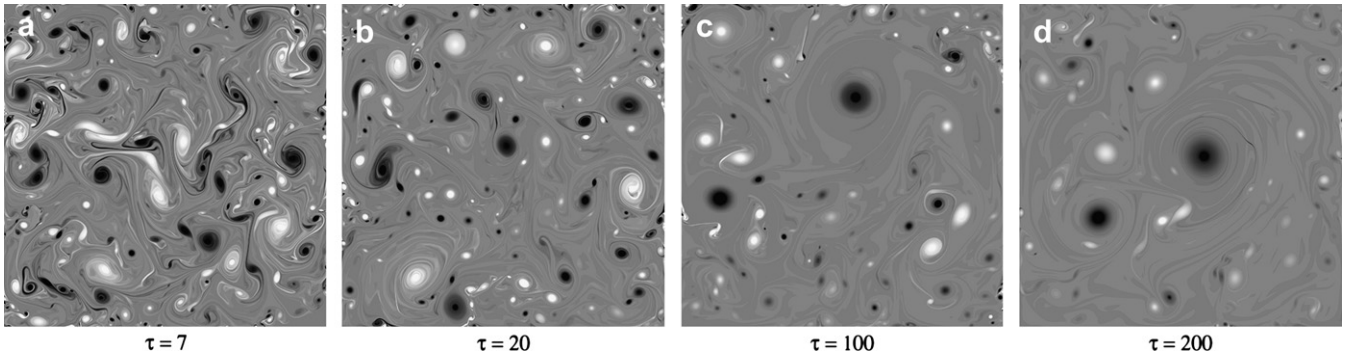

Fig. 1. Vorticity snapshots of a simulation with an initial Reynolds number $\mathrm{Re} = 10^5$. The simulation is performed with 4096^2 Fourier modes. The dimensionless time is given in terms of τ, where time has been made dimensionless by the eddy turnover time of the initial vortices positioned in an array of 10×10 vortices (position slightly distorted for breaking symmetry). Thirty grey levels are applied from $\omega = -80$ to $\omega = +80$. The normalized angular momentum is $|L| = 0.01$, 0.08, 0.28 and 0.25 for $\tau = 7$, 20, 100 and 200, respectively.

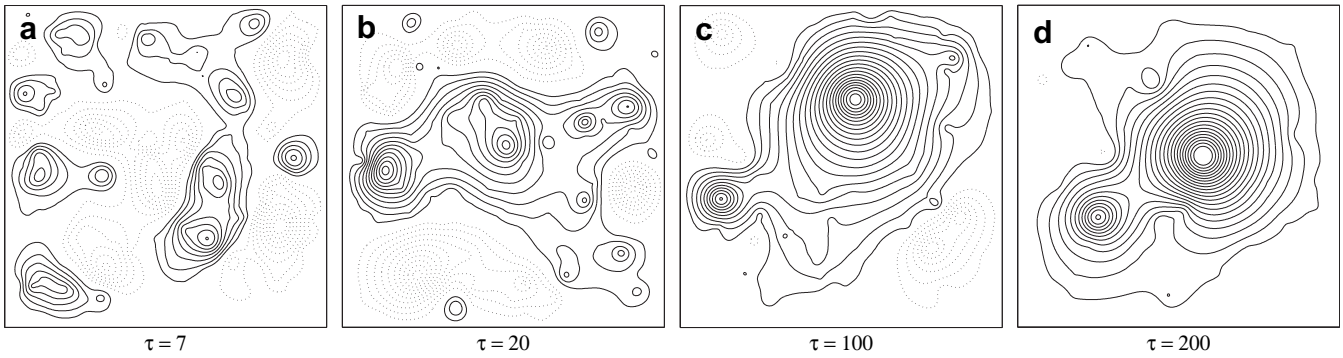

Fig. 2. Stream function plots corresponding with the vorticity fields shown in Fig. 1. Increments size is 0.04. The normalized angular momentum is $|L| = 0.01$, 0.08, 0.28 and 0.25 for $\tau = 7$, 20, 100 and 200, respectively.

As the no-slip walls serve as sources for high-amplitude vorticity the legitimacy of the classical prediction $dE/dt \propto \mathrm{Re}^{-1}$ for decaying 2D turbulence in domains enclosed by no-slip boundaries could be questioned and alternative scaling relations might be valid. Let us first recall some recent results on the scaling of vorticity production at no-slip walls. Clercx and van Heijst [18] analysed the enstrophy production during the collision of an individual dipole with a no-slip wall. They found the following scaling behaviour of the peak enstrophy: $Z_{max} \propto \mathrm{Re}^{0.75}$ for $\mathrm{Re} \lesssim 20,000$ and $Z_{max} \propto \mathrm{Re}^{0.5}$ for $\mathrm{Re} \gg 20,000$. This corresponds with an energy dissipation rate proportional to $\mathrm{Re}^{-0.25}$ and $\mathrm{Re}^{-0.5}$, respectively. It is important to realize that the Reynolds number associated with the individual vortex-wall collisions, denoted by Re_d (based on the translation speed of the vortices and the radius of the dipole half[1]), is an order of magnitude smaller than the integral-scale Reynolds number of the turbulent flow itself. For the present numerical runs we have $10 \lesssim \mathrm{Re}_d \lesssim 10^3$ and $10^2 \lesssim \mathrm{Re}_d \lesssim 10^4$ for integral-scale Reynolds numbers $\mathrm{Re} = 10^4$ and $\mathrm{Re} = 10^5$, respectively.

Fig. 4d–f reveal that the ratio of the enstrophy levels for different initial Reynolds numbers and for $\tau \gtrsim 200$ agrees quite well with the expected scaling behaviour of the enstrophy, $Z \propto \mathrm{Re}^{0.75}$ (as $\mathrm{Re}_d \ll 2 \times 10^4$). Also the amount of energy dissipation is consistent and shows a scaling which is almost proportional to $\mathrm{Re}^{-0.25}$. For example, as a rough measure of the energy dissipation rate we consider the decrease of kinetic energy δE defined with respect to the initial kinetic energy at $\tau = 400$: $\delta E \approx 1.6 \pm 0.1$, 1.3 ± 0.1 and 1.0 ± 0.1 for $\mathrm{Re} = 10^4$, 5×10^4 and 10^5, respectively. It does not satisfy the ratio 10:2:1 according to a scaling of the energy dissipation proportional to Re^{-1}. It is thus clearly shown that 2D turbulence bounded by no-slip sidewalls is strongly dissipative compared with 2D turbulence on a double periodic domain.

It may be inferred from the high-Reynolds number dipole-wall collision observations [18] that in the infinite Reynolds number limit the dissipation of kinetic energy of decaying 2D turbulence in bounded domains might eventually scale according to $\mathrm{Re}^{-0.5}$. To observe this scaling regime the integral-scale Reynolds number should, however, be one or two orders of magnitude larger such that the vortex-based Reynolds number is of the order of $\mathrm{Re}_d \approx 20{,}000$ or higher. This is left for future studies when computational resources allow this kind of numerical investigations.

Fig. 5 shows the angular momentum versus the dimensionless time τ. The run with an initial Reynolds number $\mathrm{Re} = 10^4$, see Fig. 5a, is consistent with the findings of Clercx et al. [9], who revealed a vary rapid increase of the angular momentum of the flow and a subsequent relatively slow decay during the late-time evolution.[2] The thick solid line in Fig. 5c represents the angular momentum for the run displayed in Figs. 1 and 2. The flow attains its maximum value of angular momentum around $\tau \simeq 100$, while the vorticity snapshots displayed in Fig. 1 clearly show the presence of many small-scale vortices. In some of the high-Reynolds number simulations considered here the angular momentum evolves in a similar way as for the $\mathrm{Re} = 10^4$ case. In other runs it is found that the angular momentum can show more disordered behaviour (see Fig. 5b and c). During the intermediate decay stage the flow can suddenly spin-down, presumably due to destabilization of the large-scale circulation by boundary-layer generated strong, small-scale vortices, and subsequently the flow can spin-up again. The angular momentum retains small values only briefly before it revives again. In the latter case the circulation of the large-scale flow can be in either the same or in the opposite direction. Examples of both cases are shown in Fig. 5b (opposite sign) and c (same sign). These observations are similar as found in forced 2D turbulence simulations (with much smaller integral-scale Reynolds number) [25]. After final spin-up the large-scale circulation of the flow is persistent besides a very slow overall decay on very long times.

4. Spin-up statistics

Table 2 presents the ensemble-averaged properties of the spin-up process for three different Reynolds numbers. The maximum of the angular momentum is normalized with both $L_{sb}(t = 0)$ and $L_{sb}(t)$, where $L_{sb}(t)$ is the angular momentum of the same amount of fluid, with total kinetic energy $E(t)$, in solid-body rotation. The normalization with $L_{sb}(t)$ compensates for the fact that the energy decays significantly faster for the $\mathrm{Re} = 10^4$ case compared to the two higher Reynolds number cases, see Fig. 4a. Table 2 also contains the ensemble-averaged values of the spin-up time. Three different dimensionless times have been considered based on different properties of the flow. Recall that the dimensionless time τ as used in Fig. 4 is based on the turnover time of the initial vortices. The average number of turnovers of the vortices in the domain is expected to be larger as a result of the formation of many small-scale strong vortices due to flow–wall interactions. To include this effect it is appropriate to use a different dimensionless time, and we will use the one introduced by Chasnov [26] in a study on the

[1] The typical translation speed of the vortices is based on the rms velocity of the flow, $U \approx 1$, and the range of vortex radii is obtained from the vorticity snapshots like in Fig. 1.

[2] Results from previous studies of decaying 2D turbulence in square domains with no-slip walls, computed with a 2D Chebsyhev pseudospectral method, could be reproduced with the 2D Fourier pseudospectral method with volume penalization.

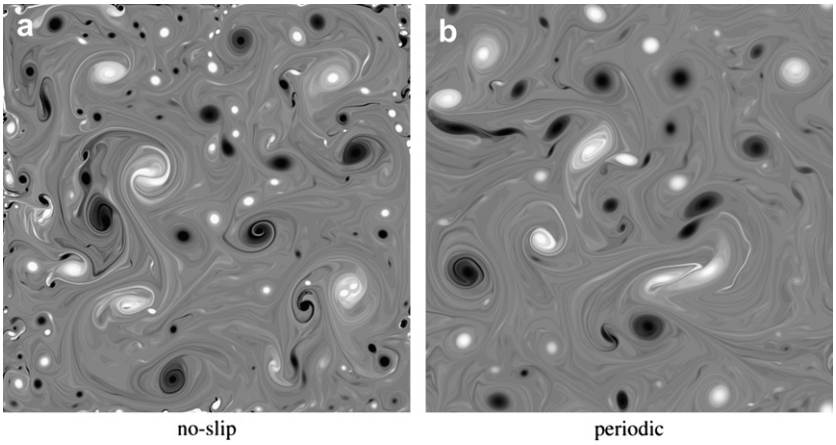

Fig. 3. Comparison of vorticity snapshots at $\tau = 15$ from two simulations with (a) no-slip and (b) periodic boundary conditions. The Reynolds number for both simulations is $\mathrm{Re} = 10^5$ and 4096^2 Fourier modes are used. The initial conditions are identical. The vorticity values range from $\omega = -80$ to $\omega = +80$ and are indicated by the grey levels. Dark grey indicates positive vorticity, light grey negative vorticity.

Reynolds number dependence of energy and enstrophy dissipation in decaying 2D turbulence on a double periodic domain,

$$\tau^* = \int_0^{t_1} \left\langle \omega^2 \right\rangle^{1/2} dt = \frac{1}{2W} \int_0^{t_1} \|\omega\|_2 \, dt = \frac{1}{\sqrt{2}W} \int_0^{t_1} \sqrt{Z} \, dt, \tag{4}$$

with W the half-width of the domain. The time τ^* can be interpreted as an appropriate measure of the turnover time of the vortices in the flow averaged over the time interval $[0, t_1]$ during which the flow acquires maximum angular momentum. It is possible to express the kinetic energy in the form of an inequality, see the Appendix, which clearly identifies τ^* as a time unit in the decay process.

A third non-dimensional time, T_g, is based on the global turnover rate of the flow, which is characterized by the rms velocity $\|\boldsymbol{u}\|_2$ (averaged over the time interval $[0, t_1]$), $T_g = 1/2W^2 \int_0^{t_1} \|\boldsymbol{u}\|_2 \, dt$. We would like to emphasize here that τ, τ^*, and T_g are all

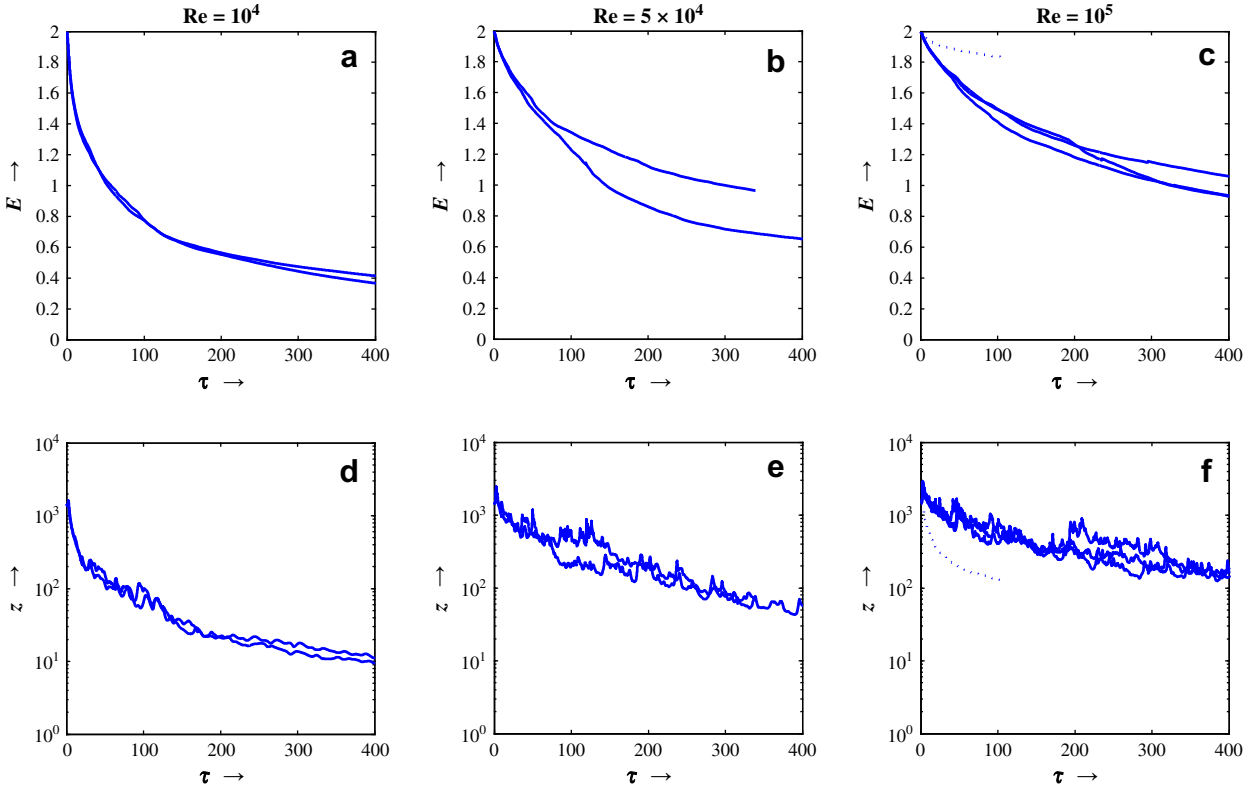

Fig. 4. The time evolution of the total kinetic energy (top row) and the enstrophy (bottom row) of decaying turbulence on a domain with no-slip boundaries versus the dimensionless time τ. Each curve represents one particular run with $\mathrm{Re} = 10^4$ (left column), $\mathrm{Re} = 5 \times 10^4$ (middle column) and $\mathrm{Re} = 10^5$ (right column). For comparison the total kinetic energy and the enstrophy for decaying flow on a double periodic domain with $\mathrm{Re} = 10^5$ are shown in the right column (dotted line). The thick solid lines in (c) and (f) correspond with the run shown in Figs. 1 and 2.

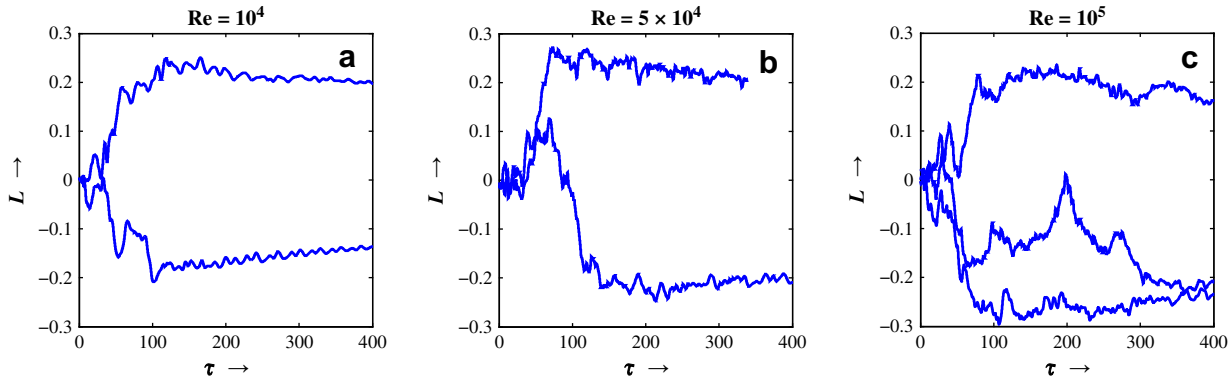

Fig. 5. The time evolution of the angular momentum normalized with $L_{sb}(\tau=0)$ for decaying turbulence on a domain with no-slip boundaries versus dimensionless time τ for $\mathrm{Re}=10^4$ (a), $\mathrm{Re}=5\times10^4$ (b) and $\mathrm{Re}=10^4$ (c). The thick solid line in (c) corresponds with the run shown in Figs. 1 and 2.

non-dimensional times (and not time scales) used for quantifying typical spin-up times for the different Reynolds number cases.

From Table 2 it can be deduced that high-Reynolds number flows show an equally strong spin-up compared with the moderate Reynolds number flows with $\mathrm{Re}=10^4$. Also the spin-up time measured in terms of the initial turnover time of the vortices τ or the global turnover time T_g does not show significant Reynolds number dependence. Note that the variation of the spin-up time between the ensemble runs is very large, see for example Fig. 5, and explains the relatively large error margins. The number of small-scale turnovers τ^* during the spin-up of the flow increases, on the other hand, with the Reynolds number. Apparently, the formation of small-scale vortices and the accompanying reduction of the overall turnover rate of the vortex population does not result in a faster spin-up of the flow for higher Reynolds numbers. This indicates that it is mainly the turnover of the dominant vortices and the associated formation of a large-scale flow pattern that determine the spin-up rate of the flow. It should, however, be mentioned here that the small-scale vortices might destabilize the large-scale circulation.

Another interesting issue is the magnitude of the torque measured by the standard deviation σ of the time-derivative of the angular momentum. The magnitude of the torque does not demonstrate significant dependence on the Reynolds number, as can be seen in Table 3. This supports the conjecture that the pressure contribution in the angular momentum balance (2) becomes finite in the high-Reynolds number limit, whereas the contribution of the viscous stresses will vanish in the same limit. It has been verified that the pressure term is at least two orders of magnitude larger than the contribution of the viscous stresses in the range $10^4 \leq \mathrm{Re} \leq 10^5$ and $\tau < 400$.

The angular momentum production during an oblique dipole-wall collision does not exhibit significant Reynolds number dependence [27]. The vortex-based Reynolds number $\mathrm{Re_d}$ of the 2D turbulence simulations considered in the present investigation is in the same order of magnitude as in Ref. [27]. Our observation that the magnitude of the torque hardly depends on the Reynolds number is thus indeed consistent with the results from oblique dipole-wall collision experiments.

5. Angular momentum production: systematic or diffusive?

In this Section we focus on the angular momentum production in the time interval between initialization of the flow and the typical time when the flow has spun up (see Table 2). The angular momentum of the flow then approaches the upper bound determined by the total kinetic energy of the flow and the shape of the domain and will subsequently decay slowly. From the time evolution of the angular momentum up to the moment the flow has spun up, shown in Fig. 5, one might be tempted to conclude that the production of angular momentum is driven by a Brownian motion like process. A more quantitative analysis of the spin-up process can be based on a comparison of the time-series of the angular momentum with a diffusion process. The test hypothesis is that the production of angular momentum is driven by stochastic fluctuations of the pressure on the domain boundaries. We will then show the incorrectness of this hypothesis.

The stochastic fluctuations of the pressure can be associated with multiple local vortex–wall interaction events (note that a full spin-up cycle requires a large number of local eddy turnover times, see Table 2, thus supporting a statistical approach). For simplicity it is assumed that the overall torque is normally distributed. The probability density function (pdf) of the local pressure of bounded 2D turbulence is not Gaussian and is strongly skewed [14]. The pressure correlation length along the domain boundary, however, is found to be small and we can then assume that the torque is the weighted sum of many statistically independent local pressure contributions

Table 2
Statistics of the spin-up variables for three different Reynolds numbers. Ensemble-averaged maximum of the absolute value of the angular momentum $\langle L_{max}\rangle$ defined as the maximum for $\tau<400$. This value is normalized with the angular momentum corresponding with solid-body rotation of the initial flow field, $L_{sb}(\tau=0)$, and based on an equivalent solid-body rotation computed with the rms velocity at the time the maximum is observed. The last three columns give the spin-up time measured in terms of the dimensionless times τ, τ^*, and T_g, respectively.

Re	$\frac{\langle L_{max}\rangle}{L_{sb}(\tau=0)}$	$\frac{\langle L_{max}\rangle}{L_{sb}(\tau)}$	τ	τ^*	T_g
10^4	0.19 ± 0.05	0.35 ± 0.07	180 ± 50	600 ± 200	45 ± 20
5×10^4	0.24 ± 0.05	0.36 ± 0.07	150 ± 50	1000 ± 300	50 ± 15
10^5	0.23 ± 0.05	0.32 ± 0.07	150 ± 50	1300 ± 500	50 ± 15

Table 3
Statistics of the torque. Standard deviation σ of the net torque, i.e. $\dot{L}$ averaged over the period $\tau<\tau_s$ where τ_s denotes the time the maximum in the absolute value of the angular momentum is observed. The standard deviation $\overline{\sigma}$ represents the torque normalized with $L_{sb}(\tau=0)$ and the turnover time of the initial vortices. The correlation time $\delta\tau_c$ estimated by the position of the first minimum of the autocovariance function of the torque.

Re	σ	$\overline{\sigma}$	$\delta\tau_c$
10^4	0.10 ± 0.01	8.1×10^{-3}	4τ
5×10^4	0.13 ± 0.02	1.1×10^{-2}	3τ
10^5	0.10 ± 0.02	8.1×10^{-3}	3τ

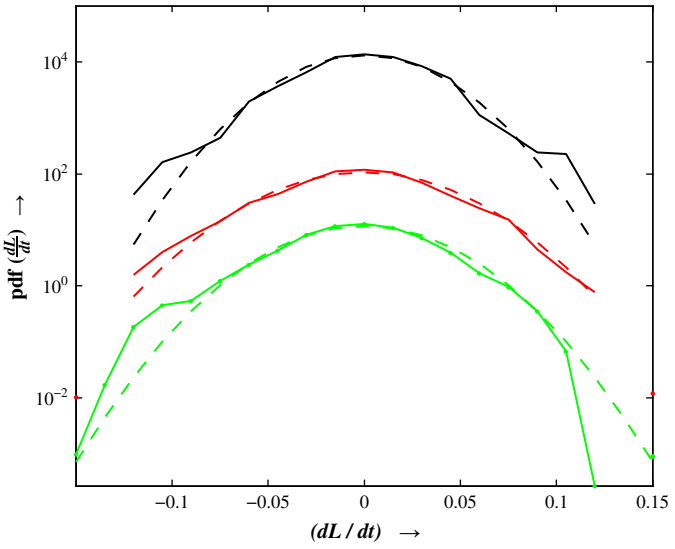

Fig. 6. Probability density function of the torque dL/dt, where L is normalized with $L_{sb}(\tau = 0)$. The pdf is computed by averaging over the simulations with initial Reynolds number of $\mathrm{Re} = 10^4$ (top), $\mathrm{Re} = 5 \times 10^4$ (middle), and $\mathrm{Re} = 10^5$ (bottom), respectively. The dashed lines represent Gaussian fits.

on the domain walls given by the same distribution. According to the central limit theorem the overall torque is then normally distributed. We have computed the pdf of the torque for three spin-up realizations, one for each Reynolds number under investigation, and the results are shown in Fig. 6. These data indeed support our assertion. Following this procedure a surrogate time-series for the angular momentum can be generated with a surrogate torque which is fully correlated for $\delta\tau < \delta\tau_c$, but independently drawn from a normal distribution for $\delta\tau > \delta\tau_c$. The statistical parameters $\delta\tau_c$ and $\overline{\sigma}$ are determined by the data reported in Table 3.

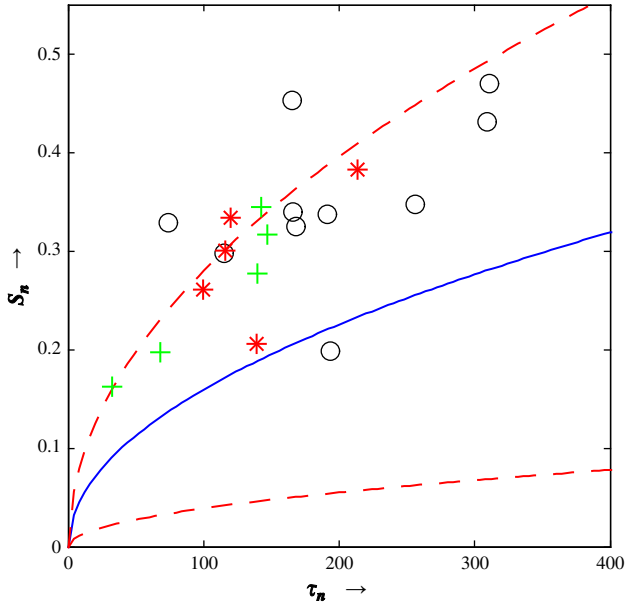

Fig. 7. Expectation value of the trace of the amplitude of a surrogate Brownian data set generated with $\delta\tau_c = 4\tau$ and $\overline{\sigma} = 8.1 \times 10^{-3}$. The solid line represent the expectation value and the dashed line the expected deviation. The markers correspond with the location in this diagram of the maximum angular momentum (normalized with $L_{sb}(\tau = 0)$) from each simulation. The different symbols represent data from runs with an initial Reynolds number of $\mathrm{Re} = 10^4$ (circles), $\mathrm{Re} = 5 \times 10^4$ (stars), and $\mathrm{Re} = 10^5$ (plusses), respectively.

The central statistical quantity considered here is the trace of a diffusion process, see for example Sprott [28]. In the present analysis the trace is expressed as $S_n = \delta\tau_c \sum_{j=1}^{n} T_j$, where T_j is drawn from the normal distribution $\mathcal{N}(0, \overline{\sigma})$ at each time level $\tau_j = j\delta\tau_c$. The expectation value for the absolute value of the trace reads $\langle |S_n| \rangle = \overline{\sigma}\delta\tau_c\sqrt{2n/\pi}$ and for the deviation we obtain $\langle (|S_n| - \langle |S_n| \rangle)^2 \rangle^{1/2} = \delta\tau_c\overline{\sigma}\sqrt{n(1 - 2/\pi)}$.

Fig. 7 shows the corresponding curves based on the observed statistics of the angular momentum and torque. The observed spin-up times and amplitudes from the simulations with $\mathrm{Re} = 10^4$ (circles), 5×10^4 (stars) and 10^5 (plusses) are also included in Fig. 7. These data points indicate that the observed spin-up rate is higher than can be expected from a standard diffusive process. The time-series of the angular momentum show persistence, *i.e.* a tendency exists to proceed a trend more strongly compared with Brownian motion. In that respect the generation of angular momentum should in our view be regarded as a systematic process, and the hypothesis is shown to be incorrect.

6. Conclusion

The high-Reynolds number simulations presented in this paper reveal that spontaneous production of angular momentum is a persistent feature of 2D turbulent flows in non-circular domains. In the lower Reynolds number regime spin-up is associated with the emergence of large-scale monopolar and tripolar structures that progressively fill the container as viscous decay continues, see Ref. [9]. Higher Reynolds number flows show strong and rapid spin-up that is statistically comparable with the lower Reynolds number cases. The angular momentum of these flows is, however, associated with a markedly different flow pattern. A large-scale circulation cell emerges early in the flow evolution that carries a dense population of high-amplitude vortices for many turnover times. High-amplitude vorticity filaments emanating from the domain boundaries are able to disrupt the internal circulation cell, but do not prevent strong spin-up events and allow the persistence of an angular momentum containing flow state. Although the boundary layers clearly affect the organization of the interior fluid, the spin-up time is not proportional to the microscopic time-scale based on the total enstrophy (and the average eddy turnover time of the vortices). Moreover, a standard diffusion process that mimics the action of local flow-wall interactions and associated pressure fluctuations cannot explain the strong and rapid spin-up of the flow. In that respect the internal flow does not merely respond to the net torque provided by local processes near boundaries alone, but exhibits an intrinsic property to relax towards an angular momentum containing large-scale flow pattern. By considering the spin-up as an intrinsic property of the internal flow it is not surprising that the macroscopic turnover time of the internal flow, based on the rms velocity and half-width of the domain, determines the spin-up rate.

In summary, the present observations suggest that spin-up should be regarded as an intrinsic and robust property of the flow that is hardly dependent on the initial Reynolds number.

Acknowledgements

We thank David Montgomery (Dartmouth, US) for many stimulating discussions and comments on our work on 2D turbulence and spontaneous spin-up phenomena during the last decade. We also thank Kai Schneider (Marseille, France) and Werner Kramer (Eindhoven, The Netherlands) for contributing to code validation and many discussions on (DNS of) 2D turbulence in domains with

no-slip sidewalls. The authors gratefully acknowledge financial support from the Dutch Foundation for Fundamental Research on Matter (FOM), which is financially supported by the Nederlandse Organisatie voor Wetenschappelijk Onderzoek (Netherlands Organization for Scientific Research, NWO). Part of this work was sponsored by the Stichting Nationale Computerfaciliteiten (National Computing Facilities Foundation, NCF) for the use of supercomputer facilities, with financial support from NWO.

Appendix. A note on the microscopic time-scale

An important time-scale in decaying turbulence is the time-scale τ^* as defined in Eq. (4). The physical interpretation of Chasnov [26] is already given in Section 4. Here we obtain an inequality that clearly demonstrates that τ^* is closely related to the decay process.

Theorem 1. The total kinetic energy $E(t)$ of viscous flow on a bounded domain $\Omega \subset \mathrm{R}^2$ with the smallest Stokes eigenvalue λ verifies for $t_1 \in (0, \infty)$ the following property

$$E(t) \leq E_0 \exp\left[-2\nu\sqrt{\lambda/E_0} \int_0^{t_1} \sqrt{Z}\, dt \right].$$

Proof: By using the Poincaré inequality $\|\boldsymbol{u}\|_2^2 \leq \lambda^{-1}\|\nabla \boldsymbol{u}\|_2^2 = \lambda^{-1}\|\omega\|_2^2$ and time-integration of $dE/dt = -2\nu Z(t)$ yields,

$$E(t) \leq E_0 \exp(-2\nu\lambda t).$$

Rewriting $dE/dt = -2\nu Z(t)$ and applying the Poincaré inequality once gives,

$$\frac{\mathrm{d}}{\mathrm{dt}} \frac{\|\boldsymbol{u}\|_2^2}{\|\boldsymbol{u_0}\|_2^2} = -2\nu \frac{\|\omega\|_2^2}{\|\boldsymbol{u_0}\|_2^2} \leq -2\nu\lambda^{1/2} \frac{\|\boldsymbol{u}\|_2}{\|\boldsymbol{u_0}\|_2} \frac{\|\omega\|_2}{\|\boldsymbol{u_0}\|_2}.$$

From the inequality $E(t) \leq E_0 \exp(-2\nu\lambda t)$ it is realized that $\|\boldsymbol{u}\|/\|\boldsymbol{u}_0\| \leq 1$ such that it follows that

$$\frac{d}{dt} \frac{\|\boldsymbol{u}\|_2^2}{\|\boldsymbol{u}_0\|_2^2} + 2\lambda^{1/2}\nu \frac{\|\omega\|_2}{\|\boldsymbol{u}_0\|_2} \frac{\|\boldsymbol{u}\|_2^2}{\|\boldsymbol{u}_0\|_2^2} \leq 0.$$

Then Gronwall's inequality in the following form finishes the proof.

Lemma 1. (Gronwall's inequality) If $\alpha(t)$ is real-valued and non-negative on $(0, \infty)$, and if the function $y(t)$ satisfies the following differential inequality:

$$\frac{dy}{dt} + \alpha(t) y \leq 0,$$

then $y(t)$ is bounded on $(0, \infty)$ by

$$y(t) \leq y(0) \exp\left(-\int_0^{t_1} \alpha(t)\, dt \right).$$

References

[1] R.H. Kraichnan, Inertial ranges in two-dimensional turbulence, Phys. Fluids 10 (1967) 1417–1423.
[2] G.K. Batchelor, Computation of the energy spectrum in two-dimensional turbulence, Phys. Fluids Suppl. 12 (1969) 233–239.
[3] C.E. Leith, Diffusion approximation for two-dimensional turbulence, Phys. Fluids 11 (1968) 671–673.
[4] W.H. Matthaeus, W.T. Stribling, D. Martinez, S. Oughton, D. Montgomery, Selective decay and coherent vortices in two-dimensional incompressible turbulence, Phys. Rev. Lett. 66 (1991) 2731–2734.
[5] G.J.F. van Heijst, H.J.H. Clercx, D. Molenaar, The effects of solid boundaries on confined two-dimensional turbulence, J. Fluid Mech. 554 (2006) 411–431.
[6] H.J.H. Clercx, G.J.F. van Heijst, Two-dimensional Navier–-Stokes turbulence in bounded domains, Appl. Mech. Rev. 62 (2009) 020802 1–25.
[7] Z. Yin, D.C. Montgomery, H.J.H. Clercx, Alternative statistical–mechanical descriptions of decaying two-dimensional turbulence in terms of "patches" and "points", Phys. Fluids 15 (2003) 1937–1953.
[8] H.J.H. Clercx, S.R. Maassen, G.J.F. van Heijst, Spontaneous spin-up during the decay of 2D turbulence in a square container with rigid boundaries, Phys. Rev. Lett. 80 (1998) 5129–5132.
[9] H.J.H. Clercx, A.H. Nielsen, D.J. Torres, E.A. Coutsias, Two-dimensional turbulence in square and circular domains with no-slip walls, Eur. J. Mech. B Fluids 20 (2001) 557–576.
[10] S.R. Maassen, H.J.H. Clercx, G.J.F. van Heijst, Self-organization of quasi-two-dimensional turbulence in stratified fluids in square and circular containers, Phys. Fluids 14 (2002) 2150–2169.
[11] S. Li, D. Montgomery, W.B. Jones, Inverse cascades of angular momentum, J. Plasma Phys. 56 (1996) 615–639.
[12] S. Li, D. Montgomery, Decaying two-dimensional turbulence with rigid walls, Phys. Lett. A 218 (1996) 281–291.
[13] S. Li, D. Montgomery, W.B. Jones, Two-dimensional turbulence with rigid circular walls, Theor. Comput. Fluid Dynam. 9 (1997) 167–181.
[14] K. Schneider, M. Farge, Decaying two-dimensional turbulence in a circular container, Phys. Rev. Lett. 95 (2005) 244502 1–4.
[15] S.R. Maassen, H.J.H. Clercx, G.J.F. van Heijst, Decaying quasi-2D turbulence in a stratified fluid with circular boundaries, Europhys. Lett. 46 (1999) 339–345.
[16] G.H. Keetels, H.J.H. Clercx, G.J.F. van Heijst, Spontaneous angular momentum generation of 2D fluid flow in an elliptic geometry, Phys. Rev. E 78 (2008) 036301 1–7.
[17] G.H. Keetels, U. D'Ortona, W. Kramer, H.J.H. Clercx, K. Schneider, G.J.F. van Heijst, Fourier spectral and wavelet solvers for the incompressible Navier–-Stokes equations with volume penalization: convergence of a dipole-wall collision, J. Comput. Phys. 227 (2007) 919–945.
[18] H.J.H. Clercx, G.J.F. van Heijst, On the dissipation of kinetic energy in 2D bounded flows, Phys. Rev. E 65 (2002) 066305 1–4.
[19] E. Arquis, J.P. Caltagirone, Sur les conditions hydrodynamique au voisinage d'une interface milieu fluide-milieu poreux: application à la convection naturelle, C. R. Acad. Sci. Paris 299 (1984) 1–4.
[20] Ph. Angot, C.-H. Bruneau, P. Fabrie, A penalization method to take into account obstacles in viscous flow, Numer. Math. 81 (1999) 497–520.
[21] G. Carbou, P. Fabrie, Boundary layer for a penalization method for viscous incompressible flow, Adv. Differ. Equ. 8 (2003) 1453–1480.
[22] G.H. Keetels, H.J.H. Clercx, G.J.F. van Heijst, A Fourier spectral solver for confined Navier–Stokes flow, Int. J. Mult. Comput. Eng. 6 (2008) 53–63.
[23] K. Schneider, M. Farge, Final states of decaying 2D turbulence in bounded domains, Physica D 237 (2008) 2228–2233.
[24] W.J.T. Bos, S. Neffaa, K. Schneider, Rapid generation of angular momentum in bounded magnetized plasmas, Phys. Rev. Lett. 101 (2008) 235003 1–4.
[25] D. Molenaar, H.J.H. Clercx, G.J.F. van Heijst, Angular momentum of forced 2D turbulence in a square no-slip domain, Physica D 196 (2004) 329–340.
[26] J.R. Chasnov, On the decay of two-dimensional homogeneous turbulence, Phys. Fluids 9 (1997) 171–180.
[27] H.J.H. Clercx, C.-H. Bruneau, The normal and oblique collision of a dipole with a no-slip boundary, Comput. Fluids 35 (2006) 245–279.
[28] J.C. Sprott, Chaos and Time-series Analysis, Oxford University Press, Oxford, United Kingdom, 2003.